

Cite this: *Green Chem.*, 2023, 25, 10458

Comparative techno-economic and life-cycle analysis of precious *versus* non-precious metal electrocatalysts: the case of PEM fuel cell cathodes†

 Angus Pedersen,[‡] Jinil Pandya,[‡] Grazia Leonzio,^{b,c} Alexey Serov,^d
 Andrea Bernardi,^{b,e} Ifan E. L. Stephens,[‡] Maria-Magdalena Titirici,^{b,f}
 Camille Petit^b and Benoît Chachuat^{b,e}

Sluggish kinetics in the oxygen reduction reaction (ORR) require significant quantities of expensive Pt-based nanoparticles on carbon (Pt/C) at the cathode of proton exchange membrane fuel cells (PEMFCs). This catalyst requirement hinders their large-scale implementation. Single atom Fe in N-doped C (Fe–N–C) electrocatalysts offer the best non-Pt-based ORR activities to date, but their environmental impacts have not been studied and their production costs are rarely quantified. Herein, we report a comparative life-cycle assessment and techno-economic analysis of replacing Pt/C with Fe–N–C at the cathode of an 80 kW PEMFC stack. In the baseline scenario (20 g_{Pt/C} vs. 690 g_{Fe–N–C}), we estimate that Fe–N–C could reduce damages on ecosystems and human health by 88–90% and 30–44%, respectively, while still increasing global warming potential by 53–92% and causing a comparable impact on resource depletion. The environmental impacts of Pt/C predominantly arise from the Pt precursor while those of Fe–N–C are presently dominated by the electricity consumption. The monetized costs of environmental externalities for both Fe–N–C and Pt/C catalysts exceed their respective direct production costs. Based on catalyst performance with learning curve analysis at 500 000 PEMFC stacks per annum, we estimate replacing Pt/C with Fe–N–C would increase PEMFC stack cost from 13.8 to 41.6 USD per kW. The cost increases despite a reduction in cathode catalyst production cost from 3.41 to 0.79 USD per kW (excluding environmental externalities). To be cost-competitive with a Pt-based PEMFC stack delivering 2020 US Department of Energy target of 1160 mW cm^{−2} (at 0.657 V), the same stack with an Fe–N–C cathode would need to reach 874 mW cm^{−2}, equivalent to a 200% performance improvement. These findings demonstrate the need for continued Fe–N–C activity development with sustainable synthesis routes in mind to replace Pt-based cathode catalyst in PEMFCs. Based on forecasting scenarios of fuel cell vehicle deployment targets, we find that Pt consumption would be constrained by Pt supply.

Received 25th August 2023,
Accepted 1st November 2023

DOI: 10.1039/d3gc03206j

rsc.li/greenchem

Introduction

The International Energy Agency predicts that for a global net zero emission scenario by 2050, 60 Mt of hydrogen will be used for power generation.¹ Hydrogen-fed fuel cells, specifically low-temperature polymer electrolyte membrane fuel cells (PEMFCs), are a promising zero CO₂ emission technology with high-technology readiness to fulfill sectors of power generation.² This is due to PEMFCs' load flexibility and therefore wide range of applications within stationary and portable power generation, and particularly transportation.² PEMFCs' rising prominence in transportation applications is supported by global Government targets of 2.5 million fuel cell electric vehicles (FCEV) on the road by 2030.³

^aDepartment of Materials, Royal School of Mines, Imperial College London, London SW7 2AZ, UK

^bDepartment of Chemical Engineering, Imperial College London, London SW7 2AZ, UK. E-mail: b.chachuat@imperial.ac.uk

^cDepartment of Mechanical, Chemical and Materials Engineering, University of Cagliari, via Marengo 2, 09123 Cagliari, Italy

^dElectrification and Energy Infrastructures Division, Oak Ridge National Laboratory, Oak Ridge, TN, USA

^eThe Sargent Centre for Process Systems Engineering, Imperial College London, SW7 2AZ London, UK

^fAdvanced Institute for Materials Research (WPI-AIMR), Tohoku University, 2-1-1 Katahira, Aobaku, Sendai, Miyagi, 980-8577, Japan

†Electronic supplementary information (ESI) available. See DOI: <https://doi.org/10.1039/d3gc03206j>

‡Angus Pedersen and Jinil Pandya have equal contributions.



egories and indicators, LCA results can be easily understood and used to guide sustainable product and process design. LCA has been applied extensively to compare the production routes of chemicals and fuels, including early-stage technologies,³⁴ but its application to catalyst production has remained scant.³⁵

Herein, we apply LCA to quantify and compare the environmental impacts of manufacturing Pt/C and Fe–N–C electrocatalysts for use in a PEMFC cathode. Of all the PEMFC stack components, such focus on the cathode electrocatalyst (Fig. 1a) is motivated by its large repercussion on PEMFC efficiency, cost, lifetime, and environmental impact, with substantial ongoing research on displacing Pt-based cathode catalyst. The two electrocatalysts are compared on a dry basis, so both ionomer and inks for depositing catalysts are ignored in the LCA. The assessment is conducted using OpenLCA 1.11 and the database ecoinvent 3.6.³⁶ The LCA comprises four phases per the ISO standards (14040:2006 and 14044:2006/AMD 2:2020): (1) goal and scope definition, (2) inventory analysis, (3) impact assessment, (4) interpretation.³⁷

Goal and scope

The goal of the LCA is to compare the environmental impacts for the manufacturing phase of Pt/C and Fe–N–C cathode electrocatalysts for an 80 kW PEMFC stack for light duty vehicle applications. The aim is to help stakeholders and policy-

makers take decisions for future investments in PEMFC cathode catalyst development, as well as informing the research community and public. Accordingly, the geographical location is chosen as the global level in the baseline scenario.

We adopt a cradle-to-gate scope for the LCA (Fig. 1b), which includes all processes from raw material extraction to the electrocatalyst production and where allocation is not required since Pt/C and Fe–N–C are the sole products. The use phase of the electrocatalysts is accounted for through setting the functional unit as the mass of cathode catalyst (grams) needed for a PEMFC stack to provide power of 80 kW at 0.657 V, including the effect of electrocatalyst amount in a *post hoc* scenario analysis. Despite Fe–N–C currently being less stable than Pt/C, Fe–N–C stability is rapidly improving¹⁴ so we make the assumption herein that Fe–N–C will eventually reach equivalent operation lifetimes to Pt/C. Regarding the end-of-life, while our baseline scenario assumes no recycling for the spent electrocatalysts, the effect of Pt recycling is investigated as part of the *post hoc* scenario analysis instead. Incorporating more details on the treatment of the spent electrocatalysts, degradation of the catalyst or PEMFC lifetime into the LCA is beyond the scope of this paper and left for future research.

The main performance characteristics of the analyzed baseline 80 kW PEMFCs are summarized in Table 1. The Pt/C cathode electrocatalyst is based on the 2020 US DOE target and performance of 0.125 mg_{Pt} cm⁻² for light duty fuel cell vehicles using PEMFC technology,^{7,38} resulting in around 20 g of Pt/C catalyst per functional unit (80 kW); refer to section A of the ESI for details.† For the Fe–N–C electrocatalyst, PEMFC performance is assumed equivalent to a Pajarito Powder Fe–N–C catalyst with 290 mW cm⁻²,¹⁷ leading to an estimated 690 g of Fe–N–C catalyst per functional unit (see section A of ESI†). The baseline scenario, therefore, compares 20 g of Pt/C against 690 g of Fe–N–C.

Life cycle inventory

Pt/C catalyst synthesis. The Pt/C synthesis process (Fig. 2a) is based on reported polyol syntheses.^{39,40} It uses chloroplatinic acid since it is the most common Pt salt precursor in the industry.⁴¹ The scale-up procedure involves mixing 40 mM chloroplatinic acid with a solution containing 0.4 M NaOH in ethylene glycol.³⁹ Next, 1 M HCl is added to the Pt colloidal solution to precipitate the nanoparticle suspension, prior to



Fig. 1 (a) PEMFC stack component hierarchy, with highlighted focus on the cathode catalyst. (b) System boundary of the PEMFC cathode electrocatalyst LCA.

Table 1 Performance, operating conditions, and components of the PEMFC stack in the baseline scenario for Pt/C and Fe–N–C. Operating temperatures and pressure are assumed to be identical in both systems (80 °C, 1 bar_g, H₂–air)

Parameter	Pt/C	Fe–N–C
Power density at 0.657 V (mW cm ⁻²)	1160	290
Cathode catalyst loading (mg _{Pt} cm ⁻² or mg _{Fe–N–C} cm ⁻²)	0.125	2.5
Active cells (–)	380	11 035
Cell active area (cm ²)	185	25
Total cathode catalyst required (g)	20	690





Fig. 2 Process diagrams with material and energy inventories to produce baseline (a) 20 g Pt/C, (b) 690 g Fe-N-C.

centrifugating the mixture three times with supernatant discarded. The recovered Pt nanoparticles are mixed with carbon black in acetone before mixing and drying. The resulting Pt/C powder is then dried in an air oven before undergoing heat activation in a furnace^{35,42} to produce the final Pt/C catalyst.

Initial lab-scale (55 mg Pt/C production) values of sodium hydroxide, ethylene glycol, chloroplatinic acid, hydrochloric acid, deionized water, and carbon black are for 50 wt% Pt/C³⁹ and adjusted to 46 wt% Pt/C, while acetone is from scaling an 8 g Pt/C lab process.⁴⁰ Energy inputs are from a previously

reported simulated 1 kg Pt/C manufacturing process,^{35,42} scaled down to 20 g, and assuming 90% efficiency of electric heat ovens and excluding the carbon support precursor processing. The reactants are scaled in stoichiometric ratios with 20% relative reduction in solvents applied during scaling.⁴³ Material losses in Pt/C production, reported to be ~3% in manufacturing quotes, are ignored. All unreacted inputs are considered waste chemicals in the outlet stream. The foreground inventories for baseline 20 g Pt/C electrocatalyst are summarized in Table 2 (left column) and reported on the

Table 2 Manufacturing inputs and outputs for Pt/C and Fe-N-C catalyst baseline scenarios

Pt/C (20 g)		Fe-N-C (690 g)	
Input	Amount	Input	Amount
Acetone (g)	768	Activated silica (kg)	1.38
Carbon black (g)	10.0	Hydrogen fluoride (kg)	2.21
Chloroplatinic acid (g)	17.7	Iron nitrate nonahydrate (kg)	0.345
Ethylene glycol (kg)	2.56	Nicarbazine (kg)	3.46
Sodium hydroxide (g)	23.3	Water, deionised (kg)	138
Water, deionised (kg)	39.7	Electricity (MJ)	5393
Hydrochloric acid (g)	318		
Electricity (MJ)	4.43		
Output	Amount	Output	Amount
Acetone, waste (g)	768	Silica, waste (kg)	1.38
Hydrochloric acid, waste (g)	318	Fe-N-C Catalyst (g)	690
Pt/C (g)	20	Hydrogen fluoride, waste (kg)	2.21
Sodium Hydroxide, waste (g)	23.3	Nicarbazine, waste (kg)	2.76
Wastewater (kg)	39.7	Wastewater (kg)	138
Ethylene glycol, waste (kg)	2.56		



process diagram in Fig. 2a (further details in Table S2†). The lack of data for chloroplatinic acid in Ecoinvent 3.6 is circumvented through creating a separate process based on literature data (eqn (S1) and Table S1†).⁷

Fe–N–C catalyst synthesis. The preparation method and reactants for the Fe–N–C electrocatalyst (Fig. 2b) is based on patents filed by the University of New Mexico.^{44–46} The N–C precursor (nicarbazin) is mixed with the Fe precursor (iron nitrate nonahydrate) and the hard template silica (Cab-O-Sil amorphous fumed) in a planetary ball mill for 1 h. Next, the mixture is pyrolysed (N_2 , 100 cc min^{-1}) at 10 °C min^{-1} up to 900 °C and held for 1.5 h, before being cooled naturally. The resulting material is washed with 25% HF for 12 h to remove the silica template, followed by subsequent washing with copious amounts of deionized water until reaching neutral pH, using a filtration pump for 4 hours. The wet material is then dried in an air oven at 85 °C for 8 h, before repeating the same pyrolysis process to form the final Fe–N–C catalyst.

All energy inputs are scaled linearly from 25 g Fe–N–C production, obtained from laboratory data (Table S5†), and by assuming that the whole production process, including large-scale furnaces, could be electrified at scale. The reactants are scaled in stoichiometric ratios and water as solvent is scaled with a 20% relative reduction.⁴³ Material losses during production are neglected, aside from during pyrolysis. Based on expert opinion and previous laboratory data from the University of New Mexico, 80% of nicarbazin precursor is assumed to be wasted in the Fe–N–C process due to the initial pyrolysis. N_2 gas flow during pyrolysis is not considered due to the low environmental impact found in OpenLCA. The amount of required HF is calculated based on the amount of silica (eqn (S2)†), with an extra 20% added to ensure complete consumption of silica. Since SiF_4 is unavailable in ecoinvent 3.6, its environmental impact is assimilated to that of HF, under the assumption of equal input and output flows of HF. All output streams other than the catalyst are treated as a waste in the baseline scenario (see Scenario subsection below). The foreground inventories for baseline 690 g Fe–N–C are summarized in Table 2 (right column) and reported on Fig. 2b (further details in Table S6†). Data for iron nitrate nonahydrate and nicarbazin are also unavailable in ecoinvent 3.6. For the former, a separate process is created, with inputs determined using weight distribution data (Table S3†). For the latter, an equimolar mix of 2-nitroaniline and 2-pyridinol is assumed to be equivalent to the nicarbazin precursor (Table S4†). Any energy inputs for producing these two precursors are furthermore omitted.

Impact assessment

Both the foreground and background inventories are translated into environmental impacts during the life-cycle impact assessment (LCIA) phase using a characterization method.^{47,48} Our assessment follows the hierarchist perspective, which is based on the cultural theory of scientific agreement and common policy principles, adopting a medium timeframe of 100 years for the environmental impacts. The LCIA method-

ology of choice is ReCiPe 2016,⁴⁹ and of the 17 midpoint indicators in ReCiPe 2016, a particular emphasis is on: *global warming potential*, caused by greenhouse gas emissions, with a reference time of 100 years per the Kyoto Protocol and Paris agreement; *fossil fuel scarcity* and *mineral resource scarcity*, to capture the depletion of both fossil and non-fossil resources; and *marine eutrophication* and *freshwater eutrophication*, to describe the enrichment of the aquatic ecosystems with nitrogenous and phosphorous compounds, respectively. Highly relevant to the present assessment are also the midpoint indicators of *acidification potential* and *human toxicity potential*, which capture the impacts of acidifying and toxic substances both on human health and on the environment. Since ReCiPe 2016 fails to account for HF in these two indicators,⁵⁰ we used CML 2001 instead in those cases.

The midpoint indicators are further aggregated into endpoint categories for three areas of protection: *human health*, expressed in terms of disability-adjusted life-years (DALY), measures the number of years that a person is disabled after a disease or accident; *ecosystem quality* measures the local species loss integrated over time (expressed in species \times year); and *resource scarcity* monetizes the burdens attributed to future mineral and fossil resource extraction (expressed in US\$ 2013). The last two endpoint indicators are quantified again using the ReCiPe 2016 methodology. To account for the impact of HF, the human health indicator is calculated by converting point units in ReCiPe 2008 to DALY in ReCiPe 2016 (world normalization factor of 73.3 and average weighting factor of 400).⁵¹ The selected characterization methods for both midpoint and endpoint impacts are summarized in Table 3.

Alongside quantifying the environmental impacts, our assessment considers their monetary valuation as externalities, or monetisation in short. This procedure translates the endpoint environmental burdens into monetary units, thereby enabling a direct comparison both between categories and with manufacturing costs. Weidema and coworkers^{52,53} first developed monetisation factors for the human health damage categories, based on the annual income generated through extending a person's life by one year, and later extended the approach by extrapolating from human health to ecosystem

Table 3 Midpoint and endpoint impact categories used

Impact	Category	Characteristic model	Units
Mid-point	Global warming potential	ReCiPe 2016	kg CO ₂ -eq
	Acidification potential	CML 2001	kg SO ₂ -eq
	Fossil resource scarcity	ReCiPe 2016	kg oil-eq
	Marine eutrophication	ReCiPe 2016	kg N-eq
	Freshwater eutrophication	ReCiPe 2016	kg P-eq
	Human toxicity potential	CML 2001	kg 1,4-DCB-eq
	Mineral resource scarcity	ReCiPe 2016	kg Cu-eq
End-point	Human health	ReCiPe 2008	DALY
	Ecosystem quality	ReCiPe 2016	species \times year
	Resource	ReCiPe 2016	USD 2013



damage. The monetisation factors (Table S7†) used herein are those by Dong *et al.*,⁵⁴ which are based on the hierarchist perspective.

Interpretation

The final phase of LCA entails interpreting the results and checking that the conclusions are well-substantiated, including uncertainty quantification and scenario analysis. Of the multiple sources of uncertainty that can affect the calculations, we focused on uncertainty in foreground inventory data since we derived the Fe–N–C process inventories from scaled-up lab procedures.⁵⁵ We also defined a range of catalyst scenarios to account for future technological advances, with a view to reducing catalyst loading and raw material use and improving production processes.

Uncertainty quantification. We conducted an uncertainty analysis through jointly propagating the uncertainty in the foreground process inputs to all the midpoint and endpoint impact indicators, using Monte Carlo analysis with 1000 Sobol samples. The uncertainty ranges of $\pm 20\%$ around the nominal process input values for both catalyst syntheses (Tables S8 and S9†) were informed by expert opinions. Due to the lack of further data, these uncertain parameters are assumed to follow triangular probability distributions.⁵⁶ In a second step, we used the same sampled scenarios in a global sensitivity analysis (GSA) to quantify how much each uncertain input contributes to the overall impact variance. We used the software SobolGSA for this, which constructs random sampling-high dimensional model representations (RS-HDMR) surrogates to compute Sobol sensitivity indices.^{57,58} Note that each uncertain input contribution adds up separately to the impact variances by construction, so the first- and total-order Sobol indices are identical and sum up to 1. Refer to section B of the ESI† for further details.

Scenario analysis. In addition to the baseline assumption of 100% virgin Pt supply, we defined two additional scenarios with 55% and 75% Pt recycling to reflect current industrial automotive Pt recycling,^{8,9} reported lab-scale results,^{28,59,60} and EU guidelines.²⁹ For simplicity, these two scenarios omit the infrastructure and energy requirements for the Pt recycling process. Therefore, the recycled Pt could also be interpreted as Pt reductions, which is in agreement with the EU's target of 71% Pt reduction by 2030 (from 2017 values).⁶¹ We considered another scenario with a reduction in Pt/C from 20 g to 15 g as Pt amounts in PEMFCs are continually reduced.⁴ On the other hand, we did not analyze any recycling scenario for Fe–N–C as it is made of cheap or abundant materials. To reflect the recent synthesis of a silica templated Fe–N–C catalyst with comparable performance yet without using any HF,⁶² we defined a separate scenario with no HF input or output. Since current Fe–N–C catalyst synthesis requires substantial amounts of electricity, we explored electricity mix based on the EU average, Poland, and Sweden, in addition to the global average electricity mix. Since production of Fe–N–C catalyst at scale would rather use a muffle furnace than a tube furnace, we considered yet another scenario that assumes the power

consumption for producing 690 g Fe–N–C with muffle furnace would be the same as producing 25 g Fe–N–C with tube furnace, which is consistent with values communicated by furnace manufacturers. Finally, we defined two scenarios of improved catalyst performance, where the required catalyst amounts were lowered to 380 g Fe–N–C and 15 g Pt/C.

Techno-economic analysis

We conducted a dynamic cost estimation based on learning curves to determine the influence of the catalyst production cost compared with other PEMFC components on the total PEMFC stack cost at varying production scales, in line with previous PEMFC production studies.^{63,64} We adopted a production rate ranging between 1000 and 500 000 stacks per year, where the lower rate is the feasible limit for automobile mass production and the upper rate represents an individual top selling automobile model.⁴¹ Note that we only considered the stack cost, while omitting the cost of the PEMFC balance of plant.

Dynamic cost estimation using learning curves. A learning curve models the human activity of accumulating knowledge or experience by cumulative production. In eqn (1), the product cost at production level i , Y_i depends on the cumulative number of products, X_i , the progress ratio, r , and a given constant A . The progress ratio r is related to the parameter F , which describes how much the production cost is reduced upon doubling the cumulative production through eqn (2).^{63,65} For instance, an F value of 80% means for the cost to be reduced by 20% each time the cumulative production volume is doubled.

$$Y_i = AX_i^{-r} \quad (1)$$

$$F = 2^{-r} \quad (2)$$

Typical values for F range between 74–95%.^{63,64} We adopt a nominal F value of 86.4% for the catalysts, which is based on baseline Fe–N–C (690 g) reaching the equivalent production cost of the 380 g Fe–N–C + muffle furnace scenario at 500 000 stacks per year. The values from Mock and Schmid⁶⁴ are applied for the rest of PEMFC components. We estimated the production costs for Pt/C and Fe–N–C from quotes from Alibaba and other relevant manufacturers, with processing costs based on calculated utility consumption and factors for plant costs from industry knowledge (Tables S10 and S11†).

For Pt/C cathode catalyst, a simple process achieving 2020 US DOE target performance is modelled with the market price of bulk precursors and electricity applied. Since the state-of-the-art de-alloyed Pt-based cathode PEMFC catalysts that meet the US DOE performance targets possess higher material and processing costs, the calculated Pt/C cathode and anode catalyst process costs are applied as the value at 500 000 stacks per year in the learning curve (Table S12†). We calculated the Pt/C anode catalyst cost assuming an equivalent production Pt/C process, but with 0.025 mg_{Pt} cm⁻² loading (cost divided by five). We based the costs of the other PEMFC components in the Pt/C system at 1000 stacks per year on previous values from



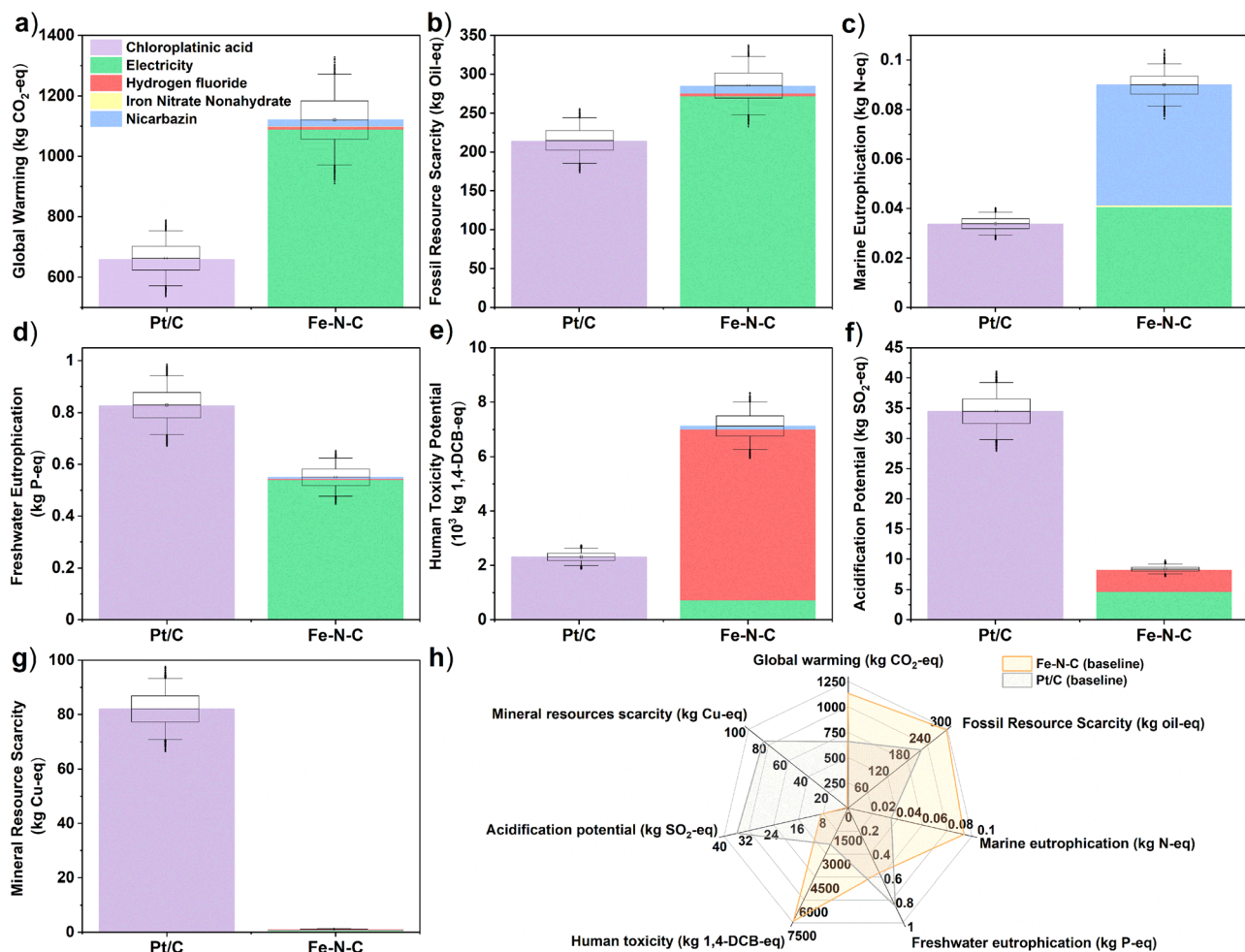


Fig. 3 Comparison of midpoint impact indicators of baseline Pt/C (20 g) and Fe-N-C (690 g). (a) Global warming potential (kg CO₂-eq). (b) Fossil resource scarcity. (c) Marine eutrophication (kg N-eq). (d) Freshwater eutrophication (kg P-eq). (e) Human toxicity potential (kg 1,4-DCB-eq). (f) Acidification potential (kg SO₂-eq). (g) Mineral resource scarcity (kg Cu-eq). The main activities contributing to each mid-point indicator are reported on each bar. The boxes on each bar represent the inter-quartile range of uncertainty scenarios, with central line showing the median and central dot the mean, and the lower and upper whiskers extending the box to the 5th and 95th percentiles, outliers represented by dots. (h) Spider chart summary of baseline Fe-N-C and Pt/C midpoint indicators.

electricity and, to a lesser extent, HF for Fe-N-C production (Table S21[†]). Though it should be noted that end-point indicators are subject to larger uncertainty than mid-indicators,⁶⁹ especially regarding uncertainties in the life-cycle (background) emissions and the LCIA characterization factors, which were not quantified here. It would thus be important, as part of future work, to study in greater depth the burden-shifting occurring between the global warming impact (greater for Fe-N-C) and both end-point impacts of human health and ecosystems quality (greater for Pt/C).

The alternative scenarios of Fe-N-C and Pt/C are compared to baseline scenarios for endpoint categories in Fig. 4d-f (see Table S22[†] for breakdown). This is complemented with a similar comparison for midpoint categories in Fig. S1[†] (with breakdown in Table S17[†]). For Fe-N-C production, the scenario with muffle furnace presents the largest improvement potential in all three damage areas of human health (-48%),

ecosystems quality (-70%) and resources (-68%). This was expected given the dominant burden of electricity consumption on Fe-N-C impacts, but nonetheless interesting that using a muffle furnace could present even greater benefits than reducing the amount of Fe-N-C catalyst to 380 g from the baseline scenario. Swapping global to EU electricity supply could also present significant environmental benefits in terms of human health (-26%), ecosystems quality (-25%) and resources (-35%) due to the reduced carbon intensity. Although this could increase both freshwater (+16%) and marine (+11%) eutrophication potentials at the mid-point level due to the higher share of brown coal (lignite) in current EU supplies compared to the global average.⁴⁹ The large impact of electricity mix on the environmental performance of Fe-N-C production is further exemplified on Fig. S2 and S3[†] (with breakdown in Tables S18 and S23[†]), where a mix with high share of renewables and low carbon intensity such as Sweden





Fig. 4 Left: comparison of endpoint impact indicators of baseline Pt/C (20 g) and Fe–N–C (690 g). (a) Human health (10^{-3} DALY). (b) Ecosystem quality (10^{-5} species \times year). (c) Resource scarcity (USD 2013). The boxes on each bar represent the inter-quartile range of uncertainty scenarios, with central line showing the median and central dot the mean, and the lower and upper whiskers extending the box to the 5th and 95th percentiles. Right: scenarios of Fe–N–C (baseline, no HF, 380 g, EU electricity) and Pt/C (baseline, 15 g, 55% and 75% Pt recycling) for endpoint categories: (d) Human health (10^{-3} DALY). (e) Ecosystem quality (10^{-5} species \times year). (f) Resources (USD 2013).

could dramatically reduce all three damage areas of human health (-76%), ecosystems quality (-72%) and resources (-81%), while a mix heavily reliant on coal such as Poland would significantly worsen the impacts on human health ($+35\%$) and ecosystems quality ($+69\%$). By contrast, the scenario without HF would bring more modest benefits, with a 16% reduction in human health impacts compared to the baseline scenario and marginal impact on other endpoints. At the midpoint level, the largest benefit of eliminating HF is on human toxicity (-88%) and acidification potential (-55%), but these two categories do not carry much weight when aggregated into the human health endpoint indicator (compare Table S19[†]). Regarding Pt/C production, reducing the amount

of catalyst or increasing Pt recycling has a very significant benefit in all environmental impact categories, which agrees with the dominant burden of chloroplatinic acid on Pt/C impacts. Within the best-case, 75% Pt recycling in particular, reductions from the baseline Pt/C scenario are close to 75% in all endpoint and midpoint impact categories. The 75% Pt recycling scenario is also more favorable than any of the Fe–N–C improvement scenarios in terms of impacts on human health and resources, although Fe–N–C still carries significantly less burden on endpoint ecosystems quality and midpoint acidification potential and mineral resource scarcity compared to any of the Pt/C scenarios. It is also noteworthy that the predicted impacts on human health and resources in the muffle



furnace scenario of Fe–N–C production remain within 20–30% of those of the optimistic 75% Pt recycling scenario, confirming the large improvement potential of Fe–N–C catalyst.

Techno-economic analysis

Material, utility, and plant costs of cathode catalysts are summarized in Tables S10 and S11.† The material costs for Fe–N–C are only 50.6 USD kg_{Fe–N–C}, with over 70% coming from the N–C precursor (nicarbazin). Meanwhile Pt/C material costs are several hundred times higher at 13 600 USD kg_{Pt/C}, with 98% of the cost from the Pt precursor (chloroplatinic acid). Normalizing material costs per kW PEMFC cathode, Fe–N–C is calculated as 0.44 USD per kW, while Pt/C is 3.39 USD per kW (Fig. S4a†). If Pt recycling was implemented the Pt/C cost could be comparable to Fe–N–C, and the material feedstock cost could also become comparable to baseline Fe–N–C if 75% Pt recycling was achieved (0.85 USD per kW). As expected from these results, Pt/C production costs show an approximate 1 : 1

ratio with feedstock price variance, while Fe–N–C is relatively insensitive (Fig. S4b†). If the price of Pt were to double, as occurred in 2008, while Fe–N–C feedstock prices remained the same, the material cost of the cathode PEMFC Pt/C would become 15-time higher than Fe–N–C. On the other hand, Fe–N–C production costs are highly sensitive to electricity price variance while Pt/C is not (Fig. S4c†).

Learning curve analysis of Pt/C and Fe–N–C is shown in Fig. 5a and b (see Tables S12 and S14† for details), with Fe–N–C and Pt/C PEMFC component breakdown shown in Fig. S5.† At 500 000 stacks per year, the Pt/C cathode makes up 25% of the PEMFC stack cost and 3.4 USD per kW, while Fe–N–C makes up only 2% of stack cost and is 0.79 USD per kW. This result relates to the total PEMFC stack cost being far lower for Pt/C than Fe–N–C cathode stacks, at 13.8 USD per kW compared to 41.6 USD per kW, respectively. This difference is caused by the 3.9-times greater required surface area of the Fe–N–C cathode system, which was assumed to increase the

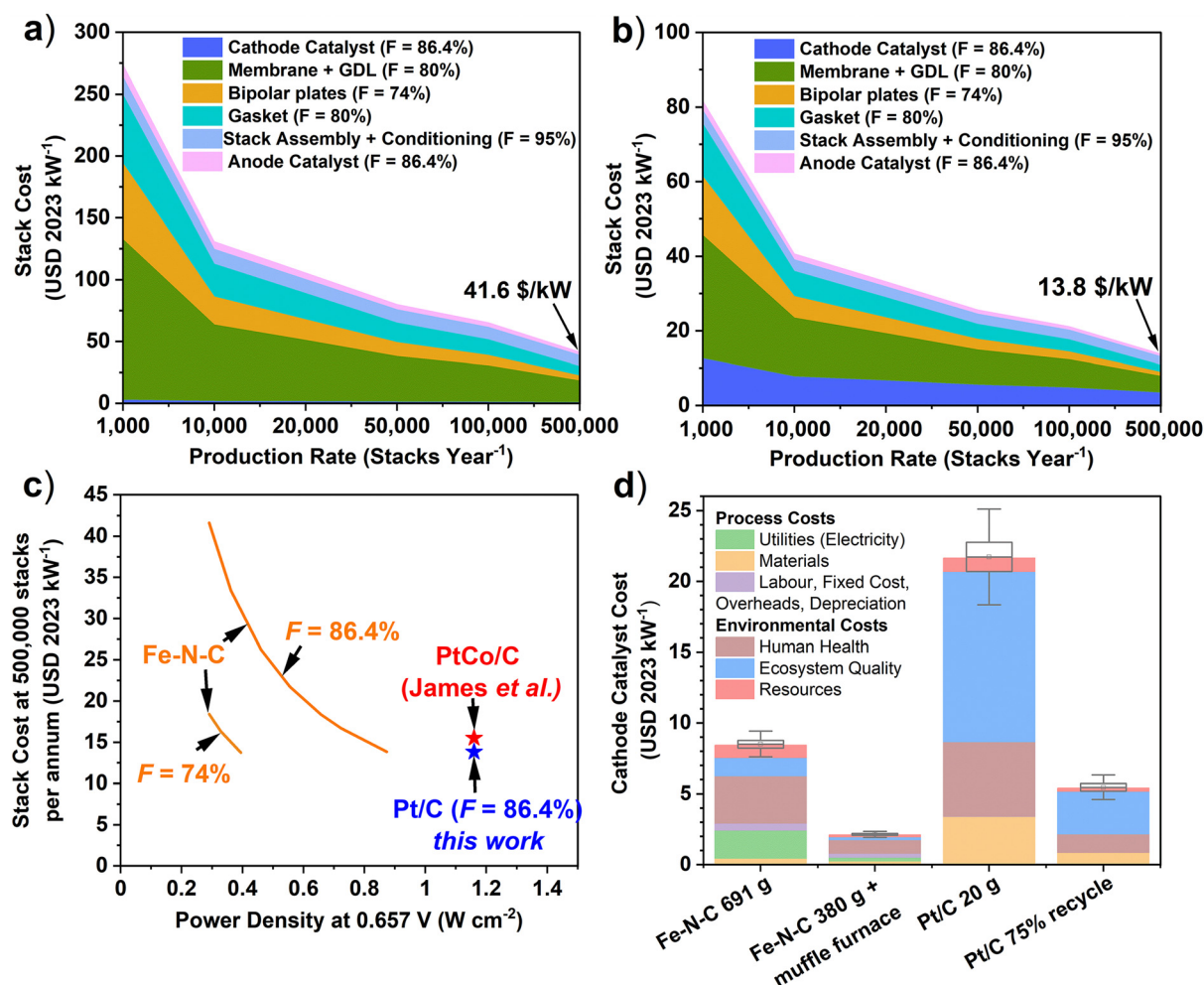


Fig. 5 Learning curve analysis of 80 kW PEMFC stack cost with production rate for baseline cathode catalysts with $F = 86.4\%$ (a) Fe–N–C (690 g_{Fe–N–C}). (b) Pt/C (20 g_{Pt/C}). (c). Variation of PEMFC stack cost at 500 000 stacks with power density for different F values for Fe–N–C compared to target Pt-based 80 kW PEMFC systems, including PtCo/C of James et al. (2018)⁷ (d) Breakdown of the total process and environmental production costs for baseline Fe–N–C (690 g_{Fe–N–C}), Pt/C (20 g_{Pt/C}), Fe–N–C 380 g_{Fe–N–C} + muffle furnace and 75% Pt recycling scenarios. Box and whisker plots are drawn using the endpoint uncertainty scenarios, with monetization applied.



J. P. Investigation: J. P., A. P., G. L. Methodology: B. C., C. P. Resource: A. S. Software: B. C., G. L., A. B. Supervision: B. C., C. P., I. E. L. S., M.-M. T. Project administration: A. P., J. P. Validation: A. P., B. C., J. P. Visualization: A. P., B. C., C. P., J. P. Writing – original draft: A. P., J. P. Writing – review & editing: all authors. A. P. and J. P. contributed equally to the article.

Conflicts of interest

There are no conflicts to declare.

Acknowledgements

A. P. thanks the EPSRC Centre for Doctoral Training in the Advanced Characterisation of Materials (grant number EP/L015277/1). B. C. and A. B. gratefully acknowledge EPSRC Funding under grants EP/V011863/1 and EP/V042432/1. A. S. gratefully acknowledges financial support from U.S. Department of Energy's Office of Energy Efficiency and Renewable Energy (EERE) under the Hydrogen and Fuel Cells Technologies Office (HFTO), FY2018 Hydrogen and Fuel Cell R&D FOA, Award Number DE-EE0008419. M.-M. T. thanks financial support from RAEng (CiET1819\2\60) and EPSRC (EP/W031019/1).

References

- International Energy Agency, *World Energy Outlook*, 2022.
- International Energy Agency, *Global Hydrogen Review 2022*, 2022.
- International Energy Agency, *The Future of Hydrogen*, 2019.
- T. Yoshizumi, H. Kubo and M. Okumura, *SAE*, 2021, **2021-01-0740**, 1–6.
- F. Jaouen, D. Jones, N. Coutard, V. Artero, P. Strasser and A. Kucernak, *Johnson Matthey Technol. Rev.*, 2018, **62**, 231–255.
- S. T. Thompson and D. Papageorgopoulos, *Nat. Catal.*, 2019, **2**, 558–561.
- B. D. James, J. M. Huya-Kouadio, C. Houchins and D. A. DeSantis, *Mass Production Cost Estimation of Direct H₂ PEM Fuel Cell Systems for Transportation Applications: 2018 Update*, 2018.
- Johnson Matthey, *PGM market report*, May, 2022.
- European Commission, *Critical Raw Materials Resilience: Charting a Path towards greater Security and Sustainability*, 2020.
- British Geological Survey, *UK criticality assessment of technology critical minerals and metals*, 2022.
- S. T. Thompson, A. R. Wilson, P. Zelenay, D. J. Myers, K. L. More, K. C. Neyerlin and D. Papageorgopoulos, *Solid State Ionics*, 2018, **319**, 68–76.
- Y. He, S. Liu, C. Priest, Q. Shi and G. Wu, *Chem. Soc. Rev.*, 2020, **49**, 3484–3524.
- L. Osmieri, J. Park, D. A. Cullen, P. Zelenay, D. J. Myers and K. C. Neyerlin, *Curr. Opin. Electrochem.*, 2021, **25**, 100627.
- S. Liu, C. Li, M. J. Zachman, Y. Zeng, H. Yu, B. Li, M. Wang, J. Braaten, J. Liu, H. M. Meyer, M. Lucero, A. J. Kropf, E. E. Alp, Q. Gong, Q. Shi, Z. Feng, H. Xu, G. Wang, D. J. Myers, J. Xie, D. A. Cullen, S. Litster and G. Wu, *Nat. Energy*, 2022, **7**, 652–663.
- B. Koyutürk, E. M. Farber, F. E. Wagner, T.-P. Fellingner and D. Eisenberg, *J. Mater. Chem. A*, 2022, **10**, 19859–19867.
- J. Feng, R. Cai, E. Magliocca, H. Luo, L. Higgins, G. L. F. Romario, X. Liang, A. Pedersen, Z. Xu, Z. Guo, A. Periasamy, D. Brett, T. S. Miller, S. J. Haigh, B. Mishra and M.-M. Titirici, *Adv. Funct. Mater.*, 2021, **31**, 2102974.
- Pajarito Powder LLC, *Active and Durable PGM-free Cathodic Electrocatalysts for Fuel Cell Application*, 2021.
- Pajarito Powder, <https://pajaritopowder.com/>, (accessed September 10, 2021).
- D. Banham, T. Kishimoto, Y. Zhou, T. Sato, K. Bai, J. I. Ozaki, Y. Imashiro and S. Ye, *Sci. Adv.*, 2018, **4**, eaar7180.
- R. Zhang, *Fuel Cells Bull.*, 2017, **2017(9)**, 55–61.
- Celcibus AB, <https://celcibus.com/>, (accessed September 30, 2023).
- M. Miotti, J. Hofer and C. Bauer, *Int. J. Life Cycle Assess.*, 2017, **22**, 94–110.
- C. Bauer, J. Hofer, H. J. Althaus, A. Del Duce and A. Simons, *Appl. Energy*, 2015, **157**, 871–883.
- R. Stropnik, A. Lotrič, A. Bernad Montenegro, M. Sekavčnik and M. Mori, *Energy Sci. Eng.*, 2019, **7**, 2519–2539.
- S. Kosai and E. Yamasue, *Sci. Total Environ.*, 2019, **651**, 1764–1775.
- M. Mori, D. Iribarren, J. Cren, E. Cor, A. Lotrič, J. Gramc, B. Drobnič, L. Rey, F. Campos-Carriedo, G. Puig-Samper, E. Bargiacchi, J. Dufour and R. Stropnik, *Int. J. Hydrogen Energy*, 2023, 1–17.
- L. Duclos, R. Chattot, L. Dubau, P. X. Thivel, G. Mandil, V. Laforest, M. Bolloli, R. Vincent and L. Svecova, *Green Chem.*, 2020, **22**, 1919–1933.
- L. Duclos, L. Svecova, V. Laforest, G. Mandil and P.-X. Thivel, *Hydrometallurgy*, 2016, **160**, 79–89.
- M. Mori, A. Lotric and R. Stropnik, *D4.3 Case studies with new strategies in dismantling and recycling stage (HyTechCycling)*, Ljubljana, 2019.
- J. Cren, J. A. Jacques, C. Paulus, R. Couturier and B. Andre, *PEGASUS: D4.1-Life Cycle Assessment*, 2021.
- H. A. Gasteiger, S. S. Kocha, B. Sompalli and F. T. Wagner, *Appl. Catal., B*, 2005, **56**, 9–35.
- B. D. James, *DOE Hydrogen and Fuel Cells Program Review Fuel Cell Vehicle and Bus Cost Analysis*, 2015.
- J. Guinée and R. Heijungs, in *Sustainable Supply Chains*, Springer, 2017, vol. 4, pp. 15–41.
- J. Kleinekorte, L. Fleitmann, M. Bachmann, A. Kätelhön, A. Barbosa-Póvoa, N. Von Der Assen and A. Bardow, *Annu. Rev. Chem. Biomol. Eng.*, 2020, **11**, 203–233.
- S. Evangelisti, C. Tagliaferri, D. Brett and P. Lettieri, in *Modern Developments in Catalysis*, World Scientific, 2017, pp. 289–312.



- 36 G. Wernet, C. Bauer, B. Steubing, J. Reinhard, E. Moreno-Ruiz and B. Weidema, *Int. J. Life Cycle Assess.*, 2016, **21**, 1218–1230.
- 37 ISO 14040, *Environmental management—life cycle assessment—principles and framework*, 2006.
- 38 US DOE - Hydrogen and Fuel Cell Technologies Office, *Hydrogen and Fuel Cell Technologies Office Multi-Year Research, Development, and Demonstration Plan. Section 3.4: Fuel Cells*, 2017.
- 39 M. Inaba, J. Quinson, J. R. Bucher and M. Arenz, *J. Visualized Exp.*, 2018, **2018**, 1–10.
- 40 M. Chourashiya, R. Sharma, S. Gyergyek and S. M. Andersen, *Mater. Chem. Phys.*, 2022, **276**, 125439.
- 41 B. D. James, J. M. Huya-Kouadio, C. Houchins and D. A. DeSantis, *Final Report: Mass Production Cost Estimation of Direct H₂ PEM Fuel Cell Systems for Transportation Applications (2012-2016)*, Strategic Analysis Inc., Golden, CO (United States), 2016.
- 42 S. Evangelisti, C. Tagliaferri, D. J. L. Brett and P. Lettieri, *J. Cleaner Prod.*, 2017, **142**, 4339–4355.
- 43 F. Piccinno, R. Hischer, S. Seeger and C. Som, *J. Cleaner Prod.*, 2016, **135**, 1085–1097.
- 44 A. Serov and P. Atanassov, *US Pat* 9673456B2, 2017.
- 45 A. Serov, B. Halevi, K. Artyushkova and P. Atanassov, *US Pat* 9515323B2, 2016.
- 46 A. Serov, B. Halevi, K. Artyushkova, P. Atanassov and M. Ulises, *US Pat* 9634 331B2, 2017.
- 47 Fuel Cell and Hydrogen - Joint Undertaking, *Guidance Document for performing LCAs on Fuel Cells and H₂ Technologies*, 2011.
- 48 R. Clift, A. Doig and G. Finnveden, *Process Saf. Environ. Prot.*, 2000, **78**, 279–287.
- 49 M. A. J. Huijbregts, Z. J. N. Steinmann, P. M. F. Elshout, G. Stam, F. Verones, M. Vieira, M. Zipp, A. Hollander and R. van Zelm, *Int. J. Life Cycle Assess.*, 2017, **22**, 138–147.
- 50 V. Aryan, M. Font-Brucart and D. Maga, *Prog. Photovolt.: Res. Appl.*, 2018, **26**, 443–459.
- 51 A. W. Sleeswijk, L. F. C. M. van Oers, J. B. Guinée, J. Struijs and M. A. J. Huijbregts, *Sci. Total Environ.*, 2008, **390**, 227–240.
- 52 B. P. Weidema, *J. Ind. Ecol.*, 2015, **19**, 20–26.
- 53 M. Pizzol, B. Weidema, M. Brandão and P. Osset, *J. Cleaner Prod.*, 2015, **86**, 170–179.
- 54 Y. Dong, M. Hauschild, H. Sørup, R. Rousselet and P. Fantke, *J. Cleaner Prod.*, 2019, **209**, 538–549.
- 55 H. A. Baaqel, A. Bernardi, J. P. Hallett, G. Guillén-Gosálbez and B. Chachuat, *ACS Sustainable Chem. Eng.*, 2023, **11**, 7157–7169.
- 56 S. Kotz and J. R. V. Dorp, *Beyond Beta: Other Continuous Families Of Distributions With Bounded Support And Applications*, World Scientific, 2004.
- 57 I. M. Sobol, *Global sensitivity indices for nonlinear mathematical models and their Monte Carlo estimates*, 2001, vol. 55.
- 58 R. S. C. Lambert, F. Lemke, S. S. Kucherenko, S. Song and N. Shah, *Math. Comput. Simul.*, 2016, **128**, 42–54.
- 59 L. Duclos, M. Lupsea, G. Mandil, L. Svecova, P.-X. Thivel and V. Laforest, *J. Cleaner Prod.*, 2017, **142**, 2618–2628.
- 60 A. Valente, D. Iribarren and J. Dufour, *Int. J. Hydrogen Energy*, 2019, **44**, 20965–20977.
- 61 Multi-Annual Work Plan 2014-2020, Fuel Cells and Hydrogen 2 Joint Undertaking, 2021.
- 62 A. Cosenza, L. Delafontaine, A. Ly, H. Wang, E. Murphy, Y. Liu, S. Specchia and P. Atanassov, *J. Power Sources*, 2023, **556**, 1–10.
- 63 H. Tsuchiya and O. Kobayashi, *Int. J. Hydrogen Energy*, 2004, **29**, 985–990.
- 64 P. Mock and S. A. Schmid, *J. Power Sources*, 2009, **190**, 133–140.
- 65 Batelle, *Manufacturing Cost Analysis of 100 and 250 kW Fuel Cell Systems for Primary Power and Combined Heat and Power Applications*, 2010, vol. 98.
- 66 Johnson Matthey, PGM prices and trading, <https://matthey.com/products-and-markets/pgms-and-circularity/pgm-management>, (accessed December 20, 2022).
- 67 T. Raymond, E. Sterck and B. Clifford, *PLATINUM ESSENTIALS Fuel cell electric vehicles are forecast to drive material long-term demand growth for platinum*, 2022.
- 68 A. B. Laursen, J. Sehested, I. Chorkendorff and P. C. K. Vesborg, *Chin. J. Catal.*, 2018, **39**, 16–26.
- 69 *Life Cycle Assessment: Theory and Practice*, in M. Z. Hauschild, R. K. Rosenbaum and S. I. Olsen, ed, Springer International Publishing, Cham, 2018.
- 70 G. Reverdiau, A. Le Duigou, T. Alleau, T. Aribart, C. Dugast and T. Priem, *Int. J. Hydrogen Energy*, 2021, **46**, 39195–39207.
- 71 K. D. Rasmussen, H. Wenzel, C. Bangs, E. Petavratzi and G. Liu, *Environ. Sci. Technol.*, 2019, **53**, 11541–11551.
- 72 L. Usai, C. R. Hung, F. Vásquez, M. Windsheimer, O. S. Burheim and A. H. Strømman, *J. Cleaner Prod.*, 2021, **280**, 125086.
- 73 R. Stropnik, N. Mlakar, A. Lotrič, M. Sekavčnik and M. Mori, *Int. J. Hydrogen Energy*, 2022, **47**, 24223–24241.
- 74 B. D. James, *Fuel Cell Cost and Performance Analysis 2022 DOE Hydrogen and Fuel Cells Program Annual Merit Review and Peer Evaluation Meeting Presentation*, 2022.
- 75 P. Boldrin, D. Malko, A. Mehmood, U. I. Kramm, S. Wagner, S. Paul, N. Weidler and A. Kucernak, *Appl. Catal., B*, 2021, **292**, 120169.
- 76 D. Banham, J. Y. Choi, T. Kishimoto and S. Ye, *Adv. Mater.*, 2019, **31**, 1–6.
- 77 G. P. Keeley, S. Cherevko and K. J. J. Mayrhofer, *ChemElectroChem*, 2016, **3**, 51–54.
- 78 M. A. Hubert, L. A. King and T. F. Jaramillo, *ACS Energy Lett.*, 2022, **7**, 17–23.

